Body-Centered Tetragonal C_{16}: A Novel Topological Node-Line Semimetallic Carbon Composed of Tetrarings

Yong Cheng, Xing Feng, Xiaoting Cao, Bin Wen, Qian Wang,* Yoshiyuki Kawazoe, and Puru Jena*

Topological semimetals have received a great deal of attention in recent years because of their fascinating physical properties and the promise in electronics applications.[1–11] Among all topological semimetals, topological semimetallic (TSM) carbon is of particular interest because of the intrinsic properties of carbon, namely, oxidation and corrosion resistance, and structural diversity. In carbon materials, 2D graphene[12] is one of the most representative TSM carbon. Considering that many practical applications often require 3D architectures built from low dimension structures,[13] much effort in recent years has been devoted to exploring 3D TSM carbon. Based on the fused hexagons form of graphene, some 3D TSM carbon allotropes have been predicted, including the Mackay–Terrones crystals (MTCs),[14] the hyperhoneycomb lattices,[15] 3D graphene networks,[16,17] and the body-centered orthorhombic C_{16} carbon (bco-C_{16}).[18] Despite this progress, the search for new 3D TSM carbon continues.

Besides hexagons that form the TSM carbon structures, recent studies on 2D carbon materials show that the other member rings can also generate TSM carbon, and bring versatile properties.[19–21] Hence, we naturally wondered if a 3D TSM carbon can be designed by taking the other member rings as the building blocks. Herein, a novel 3D carbon allotrope composed of tetrarings is proposed by means of first-principles calculations. This new carbon phase contains 16 atoms in body-centered tetragonal unit cell, and thus named bct-C_{16}. Remarkably, our calculations reveal that bct-C_{16} is a stable 3D semimetallic carbon with intriguing topological node-line state, which possesses nontrivial surface states. In addition, bct-C_{16} has bulk flat bands, which is different from the earlier proposed 3D TSM carbon. This may lead to various exotic multibody states (such as superconductivity, ferromagnetism, and Wigner crystal) by doping.[22–24]

First-principles calculations based on density functional theory (DFT)[25,26] are carried out using Vienna ab initio simulation package (VASP)[27,28] with the projector augmented wave (PAW) method[29] The generalized gradient approximation (GGA) described by Perdew et al. (PBE)[30] is adopted for the exchange-correlation potential. Moreover, the hybrid Heyd–Scuseria–Ernzerhof functional (HSE06)[31] is also employed to ensure the band structure of bct-C_{16}. The kinetic energy cutoff is taken as 500 eV, and the Monkhorst–Pack grids in Brillouin Zone (BZ) of the reciprocal space is sampled as $2\pi \times 0.02$ Å^{-1}. The conjugate-gradient algorithm is used to relax the ions, and the convergence thresholds for total energy and ionic force component are chosen as 1×10^{-6} eV and 0.001 eV Å^{-1}, respectively. The phonon frequencies are obtained using the finite displacement method implemented in the Phonopy code.[32,33] First-principles molecular dynamics (MD) simulations at different temperature are performed using the canonical (NVT) ensemble to confirm structural thermal stability. Each simulation lasts for 5 ps with a time step of 1 fs. The benchmark calculations have been performed for diamond and graphite to validate computational accuracy. The calculated results of diamond and graphite are in good agreement with the experimental and other theoretical values (see Table S1 in the Supporting Information), confirming the reliability of our computational scheme.

As shown in **Figure 1**, the structure of bct-C_{16} is a 3D carbon network, which is entirely comprised of tetrarings. After geometry optimization, bct-C_{16} is identified to possess $I4_1/amd$ space group (No. 141), and its lattice parameters are $a = b = 6.592$ Å and $c = 3.377$ Å, respectively. In the structure of bct-C_{16}, all carbon atoms are equivalent and each atom binds to other three atoms, forming two-third single bonds ($d_1 = 1.438$ Å) in tetrarings and one-third double bonds ($d_2 = 1.362$ Å) out of tetrarings. By comparing the electron density difference between bct-C_{16} and graphene (see Figure S1 in the Supporting Information), we find that, analogous to graphene, the electron distribution is symmetric

Y. Cheng, X. Feng, X. Cao, Prof. B. Wen
State Key Laboratory of Metastable Materials Science and Technology
Yanshan University
Qinhuangdao 066004, China
E-mail: wenbin@ysu.edu.cn

Prof. Q. Wang
Center for Applied Physics and Technology
College of Engineering
Peking University
Beijing 100871, China
E-mail: qianwang2@pku.edu.cn

Y. Kawazoe
New Industry Creation Hatchery Center
Tohoku University
6-6-4 Aramaki-aza-Aoba, Aoba-ku, Sendai 980-8579, Japan

P. Jena
Department of Physics
Virginia Commonwealth University
Richmond, VA 23284, USA

DOI: 10.1002/smll.201602894

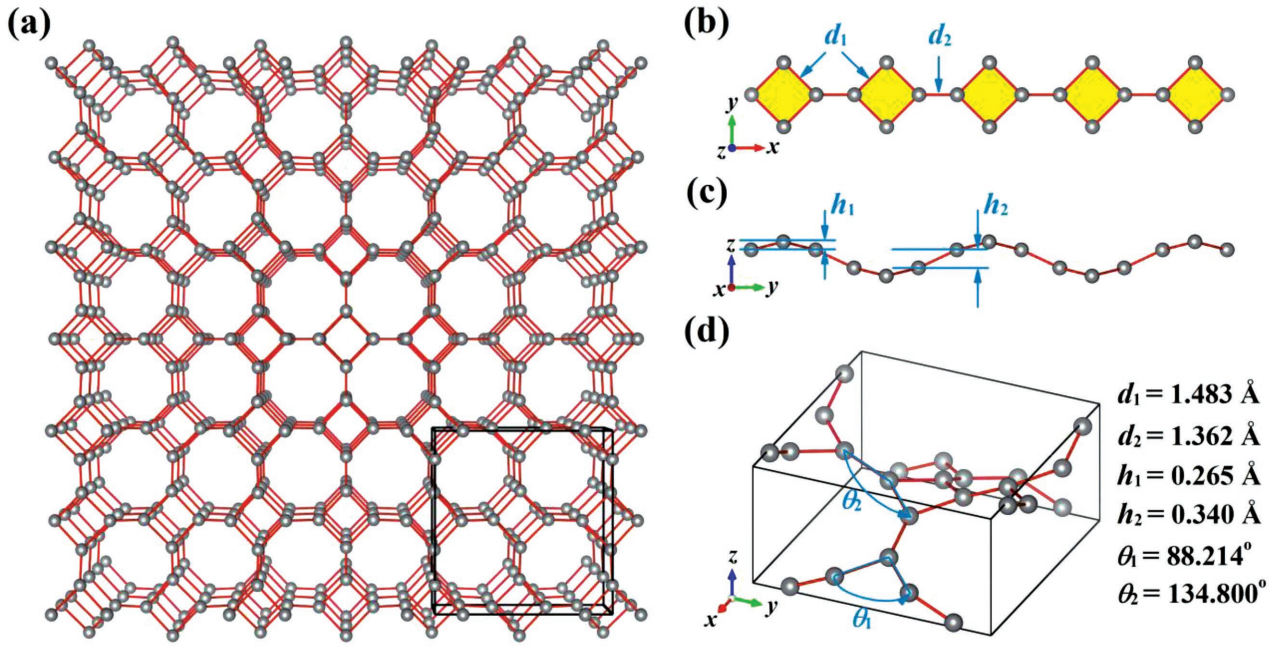

Figure 1. Schematic depiction of the structure of bct-C_{16}. a) Perspective view of the crystalline structure for bct-C_{16}. b,c) Building block of bct-C_{16} (tetraring linear chains) along *z* and *x* axis directions. d) Unit cell of bct-C_{16} composed of tetrarings with $I4_1/amd$ space group (No. 141). Its lattice parameters are $a = b = 6.592$ Å and $c = 3.377$ Å, and the Wyckoff position is 16 h (0.5, 0.34335, 0.53878).

along the double bonds in bct-C_{16}. As for the single bonds, the electron distribution is asymmetrical, showing the character of bent π hybridized bonds.[34] Therefore, bct-C_{16} also can be regarded as a twisted π hybridized network. A more detailed comparison of structural properties between bct-C_{16} and other carbon allotropes is given in Table S1 in the Supporting Information.

To verify the stability of bct-C_{16}, the total energy, phonon spectra, and elastic constants calculations as well as MD simulations have been performed. **Figure 2**a shows the calculated total energy–volume curve for bct-C_{16} and some other carbon allotropes. We find that bct-C_{16} is energetically metastable against graphite and diamond with 0.649 and 0.551 eV per atom higher in energy, respectively. This is caused by the higher ring strain in tetrarings.[35] We also note that bct-C_{16} is not only more stable than some theoretically predicted carbon allotropes (e.g., T-carbon and penta-graphene),[36,37] but also energetically more favorable than some experimentally synthesized carbon phases (e.g., C_{20} fullerene and the smallest carbon nanotube CNT(2,2)),[38–41] implying that the bct-C_{16} could be synthesized. Figure 2b displays the phonon spectra of bct-C_{16} at zero pressure, where the absence of imaginary frequencies throughout the entire BZ implies that bct-C_{16} is dynamically stable. The highest phonon frequency of bct-C_{16} is calculated to be about 1691 cm^{-1} at Γ point, which is higher than that of graphite (≈1600 cm^{-1}).[42] A wide

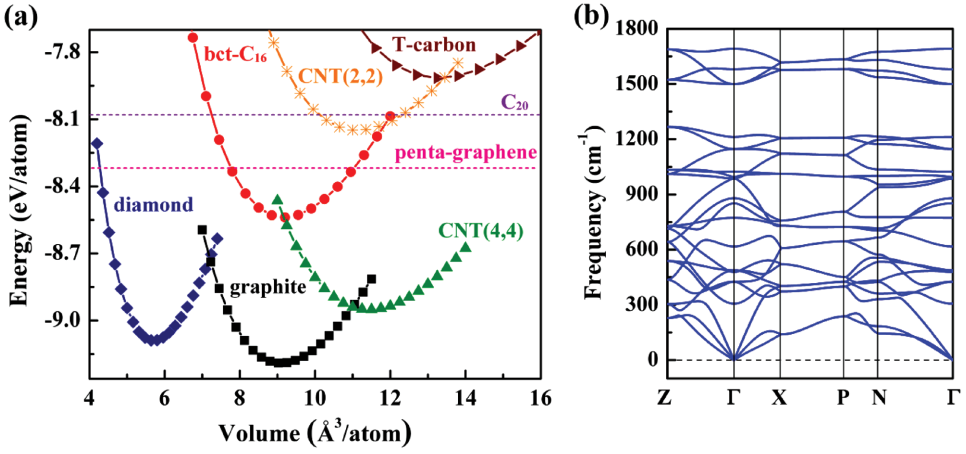

Figure 2. Energetic and dynamical stability of bct-C_{16}. a) Total energy per atom as a function of volume for some 3D carbon allotropes including bct-C_{16}, graphite, diamond, CNT(4,4), CNT(2,2), and T-carbon, as well as the total energy per atom of 2D penta-graphene and 0D C_{20} fullerene molecule. The corresponding total energies for these allotropes are –8.539, –9.188, –9.090, –8.951, –8.149, –7.916, –8.319, –8.081 eV per atom, respectively. b) Phonon spectra of bct-C_{16} at zero pressure.

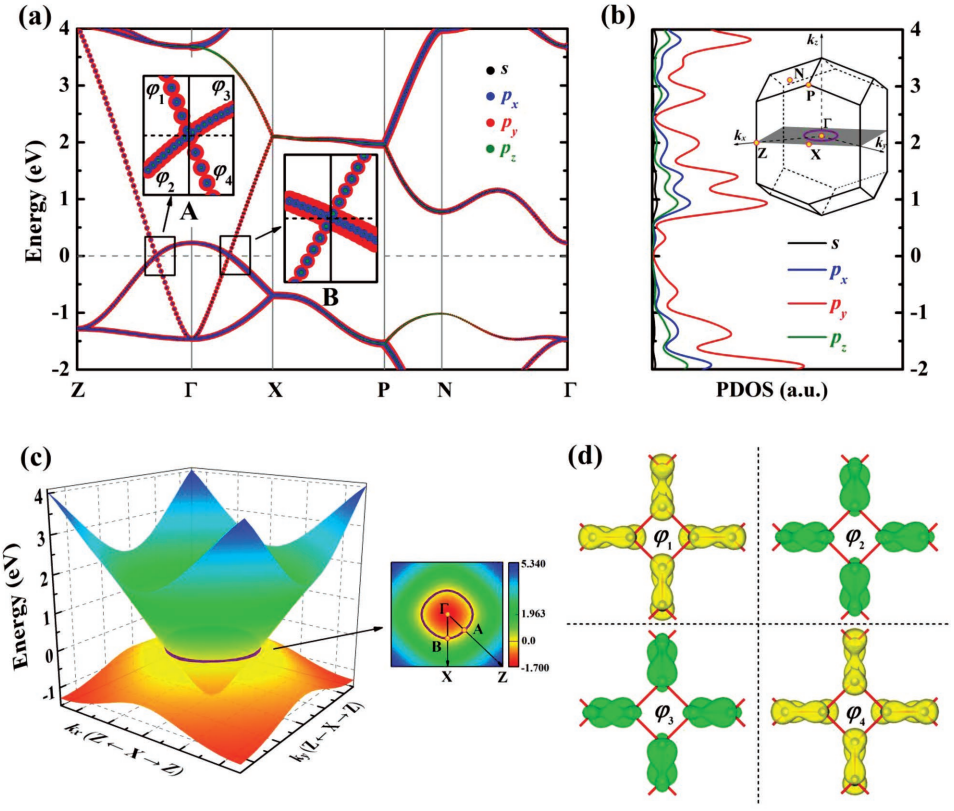

Figure 3. Node-line in bct-C_{16} without SOC. a) Orbital projection band structure of bct-C_{16}, where the black, blue, red, and olive solid circles correspond to s, p_x, p_y, and p_z orbitals of carbon, respectively. The insets show the zoom-in band structure around *A* and *B* crossing points. b) Relevant PDOS of bct-C_{16}, the Fermi level is set to zero. The inset shows the BZ of bct-C_{16}, the node-line is schematically shown with purple circle, which surrounds the *Γ* point and lies on the *Z*–*Γ*–*X* plane (gray mirror plane). c) The lotus-root-like Fermi surface (left) and the node-line (right) formed by cross points in the *Z*–*Γ*–*X* plane. d) φ_1–φ_4 show the band-decomposed charge densities of the HVB and LCB near the *A* point as indicated in inset of (a), the isosurface of the bonding charge density is 0.016 e bohr^{-3}.

indirect phonon gap of about 232 cm^{-1} can be observed in the region of *Z* to *Γ* point. These results could be helpful to identify the bct-C_{16}. As it belongs to tetragonal crystal system, the bct-C_{16} phase has six independent elastic constants, i.e., C_{11}, C_{33}, C_{44}, C_{66}, C_{12}, and C_{13}, which are calculated to be 589, 87, 54, 150, 307, 77 GPa, respectively. Obviously, these values satisfy Born criteria for tetragonal phase:[43] $C_{11} - C_{12} > 0$, C_{11}, C_{33}, C_{44}, $C_{66} > 0$, $C_{11} + C_{33} - 2C_{13} > 0$, and $2C_{11} + C_{33} + 2C_{12} + 4C_{13} > 0$, confirming that bct-$C_{16}$ is mechanically stable. Using Voigt–Reuss–Hill approximation,[44] the bulk and shear modulus (*B* and *G*) of bct-C_{16} are calculated to be 165 and 87 GPa, respectively, which are much lower than that of diamond.[45] The relatively high *B*/*G* ratio in bct-C_{16} implies that bct-C_{16} is ductile according to the Paugh criterion.[46] From the results of the first-principles MD simulations, using a large supercell of 2 × 2 × 4, we find that the skeleton of bct-C_{16} remains nearly intact after heating it at 300 and 1000 K for 5 ps, respectively, and the total energy fluctuations are very small in both cases (see Figure S2 in the Supporting Information). These results indicate that bct-C_{16} is thermally stable at room temperature, and once synthesized, bct-C_{16} can withstand temperatures up to 1000 K.

After confirming the structural stability of bct-C_{16}, we turn to investigate its electronic properties. The band structure of bct-C_{16} is presented in **Figure 3**a. It can be seen that the highest valence band (HVB) and the lowest conduction band (LCB) cross near the Fermi level, showing a feature of Dirac linear dispersion. The two crossing points are located at asymmetric *A* and *B* points along the *Z*–*Γ* and *Γ*–*X* paths, and roughly deviate from the Fermi level with an energy about 17 and 3 meV, respectively [see the inset in Figure 3a]. From Figure 3b, one can note that the density of states of bct-C_{16} is almost zero at the Fermi level. These results suggest that the bct-C_{16} is semimetallic. We also note that the band structure of bct-C_{16} has almost no change and only shifts 0.25 eV above the Fermi level when using the HSE06 functional (see Figure S3 in the Supporting Information), indicating that the feature of Dirac linear dispersion in bct-C_{16} is robust. To more clearly reveal the linear dispersion relation in reciprocal space, the 3D band structure of bct-C_{16} has been calculated, as plotted in Figure 3c. It can be seen that the crossing of HVB and LCB leads to a lotus-root-like Fermi surface in the 3D BZ, and the crossing points form a node-line rather than multiple degenerate node points in the *Z*–*Γ*–*X* plane. Due to the tetragonal symmetry, there is only one node-line in the BZ of bct-C_{16} [see the inset in Figure 3b], which is distinct from the cubic symmetric MTCs[14] that has three node-lines. Hence, the bct-C_{16} is a new type of topological node-line semimetal, and the node-line is protected by time-reversal and spatial inversion symmetries. More

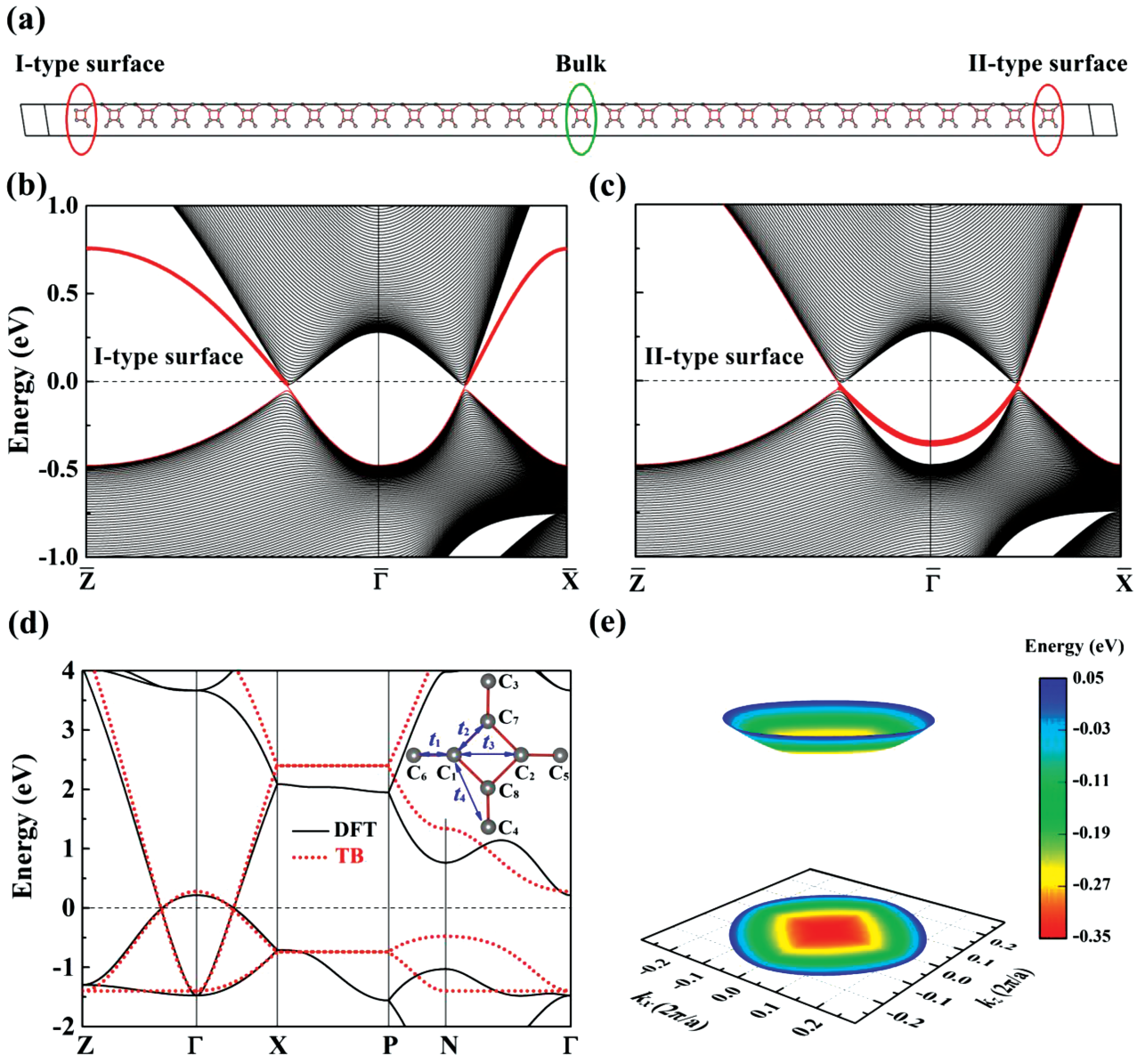

Figure 4. Surface states of bct-C_{16}. a) Atomic structure of bct-C_{16} for two types of (001) surface. b,c) I-type surface states (outside the node-line) and II-type surface states (inside the node-line). d) Comparison of band structure from DFT calculations (black line) and TB (red circle) model. The inset shows the TB model for bct-C_{16} with hopping parameter $t_1 = 3.0$ eV, $t_2 = 2.7$ eV, $t_3 = -1.6$ eV, $t_4 = 0.13$ eV. e) 3D view corresponds to the II-type surface states nested inside the node ring.

interestingly, it is also noted that there exists bulk flat bands along the *X*–*P* path at ≈2 eV. If shifting the Fermi level to pass through the flat band by electron doping, the Dirac and flat bands coexist in bct-C_{16}, which may lead to some fascinating multi-body states.[47] In addition, the Fermi velocities (vF) of bct-C_{16} have been also evaluated by fitting the slope of HVB and LCB. Along the *Z*–*Γ* direction, the vF for the HVB and LCB are 8.5×10^5 and 2.3×10^5 m s^{-1}, respectively. Along the *Γ*–*X* direction, the vF for the HVB and LCB are 7.5×10^5 and 1.9×10^5 m s^{-1}, respectively. So the carriers in bct-C_{16} are highly anisotropic. In particular, these values are in the same magnitude compared with Fermi velocity of graphene (present calculations value: 8.4×10^5 m s^{-1}, other theoretical value: 8.22×10^5 m s^{-1} and 8.6×10^5 m s^{-1}).[48,49]

To understand the origin of the lotus-root-like Fermi surface, the partial density of states (PDOS) projected to different atomic orbitals and the band decomposed charge density have been calculated. From the PDOS in Figure 3b, we note that the electronic states near Fermi level mainly originate from the p orbitals, especially p_y orbitals, which account for about 68% the orbital contributions. Thus, it can be inferred that the interactions between the p_x, p_y, and p_z orbitals result in the formation of the π and π^* bands near the Fermi level, which lead to the emergence of lotus-root-like Fermi surface in low-energy electronic structure. This is different from the origin of Dirac cone of graphene, whose π and π^* bands are attributed to p_z orbitals exclusively.[12] Figure 3d shows the charge densities [φ_1–φ_4, see the inset of

Figure 3a] in HVB and LCB around the *A* point. Note that the distributions of charge are very similar and roughly parallel to the C—C bonds, showing the character of π bonds derived primarily from the p orbitals. These results further confirm the discussions in PDOS. Remarkably, there still exists slight difference between the charge distributions of φ_1 (φ_4) and φ_2 (φ_3), implying that the HVB and LCB are inversed at the two sides of the *A* point. This band inversion also occurs at the two sides of the *B* point, and is believed to induce the behavior of band crossing near the Fermi level.

Due to the existence of band inversion and node-line, the bct-C_{16} should have nontrivial surface states. In order to capture the characters of these surface states, we use a simple tight-binding (TB) model of π-electrons to describe the band structure in the proximity of the Fermi level for bct-C_{16}. The TB model is written as

$$H = \sum_{\langle ij \rangle} t_{ij} c_i^+ c_j + \text{hc}$$

where *i* and *j* are the orbitals sites, t_{ij} is the hopping parameter between the *i*-th and *j*-th sites, c_i^+ and c_j represent the creation and annihilation operators of an electron at the site *i* and *j*, respectively. For t_{ij}, as shown in the inset of **Figure 4**d, the nearest-neighbor hopping and the second-nearest-neighbor hopping are considered in the primitive cell of bct-C_{16}. The distance-dependent hopping parameters are t_1 = 3.0 eV, t_2 = 2.7 eV, t_3 = –1.6 eV, t_4 = 0.13 eV, respectively. By diagonalizing an 8 × 8 matrix in the reciprocal space, the TB band structure is obtained, as illustrated in Figure 4d. One can see that the TB band structure agrees well with the DFT band structure in the proximity of the Fermi level, especially along the *Z*–*X* path, demonstrating that this simple TB model is good enough to describe the low energy band structure of bct-C_{16}. As presented in Figure 4a, depending on the termination of plane, bct-C_{16} has two different (001) surfaces, say, I-type and II-type surfaces. Using the above TB model, the band structure of a thick slab for the two type surfaces has been calculated, and the results are plotted in Figure 4b,c, respectively. It can be observed that the surface flat bands are located outside the node ring for I-type surface, while they emerge inside the node ring for II-type surface. In particular, we obtain that the Berry phase (a Z_2-type invariant) of I-type surface equals π for $k_{||}$ (any in-plane momentum) outside the node ring, while the Berry phase of II-type surface is π for $k_{||}$ inside the node ring. This nonzero quantized Berry phase is believed to result in the surface flat bands inside or outside the node ring. These flat bands could give rise to interesting electron interaction effects and transport physics,[3–5,9,14,16] and the drumhead-like surface states in Figure 4e can be easily detected by angle-resolved photoelectron spectroscopy or scanning tunneling microscopy.

To study the possible topological phase transition in bct-C_{16}, the spin–orbit coupling (SOC) is taken into account in our DFT calculations. As a benchmark, the band structure of graphene with SOC is calculated, we find that the bandgap at Dirac point is only 0.008 meV, which is identical to the value of previous works.[50] In the same way, the band structure of bct-C_{16} with SOC is also calculated, and the results are depicted in Figure S4 in the Supporting Information. Note that the two bandgaps of 0.76 and 0.96 meV are opened at the *A* and *B* points by SOC, respectively. Although these values are much larger than that of graphene, the influences of SOC for bct-C_{16} are still considerably weak, and can be neglected at temperatures higher than 11 K, implying that the topological node-line state in bct-C_{16} is robust, unless either one of the time-reversal and spatial inversion symmetry is broken or both are simultaneously broken.

To guide experimental observation, the X-ray diffraction (XRD) patterns of bct-C_{16} with wavelength 1.5406 Å are simulated. The results are plotted in **Figure 5**, where they are compared with those of graphite, diamond, bco-C_{16}, as well as the experimental data from the detonation soot.[51] One can see that two strong peaks at 2θ = 27.0° and 29.7° correspond to the bct-C_{16} (11) and (100) diffraction, respectively, which are different from the diamond (111) diffraction at 43.8°, but very close to the graphite (002) diffraction at 26.2° and bco-C_{16} (101) diffraction at 29.2°. Remarkably, similar to the bco-C_{16} (101) diffraction, our simulated XRD patterns show that the (100) diffraction peak of bct-C_{16} also perfectly matches the 30° diffraction peak in the detonation soot, which do not correspond to any previously known carbon phases. These results suggest that bct-C_{16} is a likely candidate structure for the unknown carbon phase in the detonation soot. Since the basic building block of bct-C_{16} is tetraring, the cyclobutadiene (the simplest carbon four-membered ring organic molecule: C_4H_4) can be considered as a precursor to synthesize the fascinating bct-C_{16} phase via the

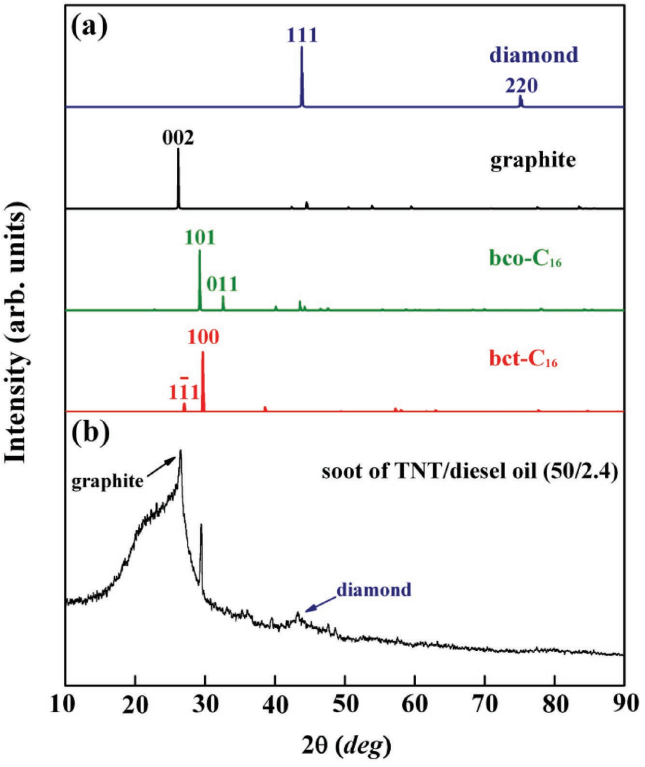

Figure 5. X-ray diffraction (XRD) patterns. a) Simulated XRD patterns of bct-C_{16} compared with diamond, graphite, and bco-C_{16}, the XRD wavelength is 1.5406 Å. b) Experimental XRD patterns for detonation soot.[51]

dehydrogenation. This is analogous to the CNTs synthesized directly by using dehydrogenated benzene molecule.[52,53] Indeed, our calculated energy results confirm that the dehydrogenation process of C_4H_4 (4 C_4H_4 (–46.557 eV per molecule) → bct-C_{16} (–136.619 eV per unit cell) + 8 H_2 (–6.771 eV per molecule)) is an exothermic reaction, implying that the suggested method is thermodynamically allowed. In addition, we also note that there is a negative slope (k_1 = –0.203) of the tangential line between the energy–volume curves of bct-C_{16} and CNT(4,4) (see Figure S5 in the Supporting Information for details), suggesting that the bct-C_{16} could be also formed from CNT(4,4) via pressure (about 32.5 GPa) induced structural phase transition.[54]

In conclusion, we predict a new body-centered tetragonal carbon allotrope named the bct-C_{16} that consists of tetrarings. The results of total energy, phonon spectra, and elastic constants as well as molecular dynamics simulations indicate that although the bct-C_{16} phase is energetically metastable as compared to graphite and diamond, it is dynamically and mechanically stable at zero pressure and room temperature, and it can withstand temperature up to 1000 K. Both first-principles calculations and TB model study of electronic band structure confirm that bct-C_{16} is a 3D topological node-line semimetal with bulk flat bands, and the SOC in bct-C_{16} is very weak and does not affect the flat surface states, making bct-C_{16} topologically robust. Our work not only predicts the existence of 3D topological semimetallic carbon allotropes consisting of other member rings, but also provides a likely crystalline structure for the unknown phase produced in the detonation soot.

Supporting Information

Supporting Information is available from the Wiley Online Library or from the author.

Acknowledgements

This work was supported by the National Natural Science Foundation of China (NSFC-51372215 and NSFC-51471004). P.J. acknowledges support of the U. S. Department of Energy, Office of Basic Energy Sciences, Division of Materials Sciences and Engineering under Award #DE-FG02-96ER45579. The authors would like to thank the staff of the Center for Computational Materials Science, Institute for Materials Research, Tohoku University for computer support.

[1] Z. Liu, B. Zhou, Y. Zhang, Z. J. Wang, H. Weng, D. Prabhakaran, S.-K. Mo, Z. Shen, Z. Fang, X. Dai, *Science* **2014**, *343*, 864.
[2] Z. K. Liu, J. Jiang, B. Zhou, Z. J. Wang, Y. Zhang, H. M. Weng, D. Prabhakaran, S. K. Mo, H. Peng, P. Dudin, T. Kim, M. Hoesch, Z. Fang, X. Dai, Z. X. Shen, D. L. Feng, Z. Hussain, Y. L. Chen, *Nat. Mater.* **2014**, *13*, 677.
[3] Y. Kim, B. J. Wieder, C. L. Kane, A. M. Rappe, *Phys. Rev. Lett.* **2015**, *115*, 036806.
[4] R. Yu, H. Weng, Z. Fang, X. Dai, X. Hu, *Phys. Rev. Lett.* **2015**, *115*, 036807.
[5] J. Zhao, R. Yu, H. Weng, Z. Fang, arXiv:1511.05704.
[6] S. Y. Xu, C. Liu, S. K. Kushwaha, R. Sankar, J. W. Krizan, I. Belopolski, M. Neupane, G. Bian, N. Alidoust, T. R. Chang, H. T. Jeng, C. Y. Huang, W. F. Tsai, H. Lin, P. P. Shibayev, F. C. Chou, R. J. Cava, M. Z. Hasan, *Science* **2015**, *347*, 294.
[7] B. Q. Lv, H. M. Weng, B. B. Fu, X. P. Wang, H. Miao, J. Ma, P. Richard, X. C. Huang, L. X. Zhao, G. F. Chen, Z. Fang, X. Dai, T. Qian, H. Ding, *Phys. Rev. X* **2015**, *5*, 031013.
[8] Z. Liu, L. Yang, Y. Sun, T. Zhang, H. Peng, H. Yang, C. Chen, Y. Zhang, Y. Guo, D. Prabhakaran, *Nat. Mater.* **2016**, *15*, 27.
[9] G. Bian, T.-R. Chang, R. Sankar, S.-Y. Xu, H. Zheng, T. Neupert, C.-K. Chiu, S.-M. Huang, G. Chang, I. Belopolski, *Nat. Commun.* **2016**, *7*, 10556.
[10] J. Ruan, S.-K. Jian, D. Zhang, H. Yao, H. Zhang, S.-C. Zhang, D. Xing, *Phys. Rev. Lett.* **2016**, *116*, 226801.
[11] C. Fang, L. Lu, J. Liu, L. Fu, *Nat. Phys.* **2016**, *12*, 337.
[12] A. C. Neto, F. Guinea, N. Peres, K. S. Novoselov, A. K. Geim, *Rev. Mod. Phys.* **2009**, *81*, 109.
[13] C. Li, G. Shi, *Nanoscale* **2012**, *4*, 5549.
[14] H. Weng, Y. Liang, Q. Xu, R. Yu, Z. Fang, X. Dai, Y. Kawazoe, *Phys. Rev. B* **2015**, *92*, 045108.
[15] K. Mullen, B. Uchoa, D. T. Glatzhofer, *Phys. Rev. Lett.* **2015**, *115*, 026403.
[16] Y. Chen, Y. Xie, S. A. Yang, H. Pan, F. Zhang, M. L. Cohen, S. Zhang, *Nano Lett.* **2015**, *15*, 6974.
[17] C. Zhong, Y. Chen, Y. Xie, S. A. Yang, M. L. Cohen, S. Zhang, *Nanoscale* **2016**, *8*, 7232.
[18] J.-T. Wang, H. Weng, S. Nie, Z. Fang, Y. Kawazoe, C. Chen, *Phys. Rev. Lett.* **2016**, *116*, 195501.
[19] J. Wang, H. Huang, W. Duan, Z. Liu, *J. Chem. Phys.* **2013**, *139*, 184701.
[20] L.-C. Xu, R.-Z. Wang, M.-S. Miao, X.-L. Wei, Y.-P. Chen, H. Yan, W.-M. Lau, L.-M. Liu, Y.-M. Ma, *Nanoscale* **2014**, *6*, 1113.
[21] L. Zhang, Z. Wang, Z. M. Wang, S. Du, H.-J. Gao, F. Liu, *J. Phys. Chem. Lett.* **2015**, *6*, 2959.
[22] N. Shima, H. Aoki, *Phys. Rev. Lett.* **1993**, *71*, 4389.
[23] K. Shiraishi, H. Tamura, T. Kimura, H. Takayanagi, *Phys. Rev. B Condens. Matter Mater. Phys.* **2002**, *65*, 085324.
[24] N. B. Kopnin, T. T. Heikkila, G. E. Volovik, *Phys. Rev. B: Condens. Matter Mater. Phys.* **2011**, *83*, 220503.
[25] P. Hohenberg, W. Kohn, *Phys. Rev.* **1964**, *136*, B864.
[26] W. Kohn, L. J. Sham, *Phys. Rev.* **1965**, *140*, A1133.
[27] G. Kresse, J. Furthmüller, *Phys. Rev. B* **1996**, *54*, 11169.
[28] G. Kresse, D. Joubert, *Phys. Rev. B* **1999**, *59*, 1758.
[29] P. E. Blöchl, *Phys. Rev. B* **1994**, *50*, 17953.
[30] J. P. Perdew, K. Burke, M. Ernzerhof, *Phys. Rev. Lett.* **1996**, *77*, 3865.
[31] G. E. Scuseria, J. Heyd, M. Ernzerhof, *J. Chem. Phys.* **2003**, *118*, 8207.
[32] Q. Li, Y. M. Ma, A. R. Oganov, H. B. Wang, H. Wang, Y. Xu, T. Cui, H. K. Mao, G. T. Zou, *Phys. Rev. Lett.* **2009**, *102*, 175506.
[33] A. Togo, F. Oba, I. Tanaka, *Phys. Rev. B* **2008**, *78*, 134106.
[34] M. Hu, X. Dong, Y. Pan, B. Xu, D. Yu, J. He, *J. Phys.: Condens. Matter* **2014**, *26*, 235402.
[35] G. Long, Y. Zhou, M. Jin, B. Kan, Y. Zhao, A. Gray-Weale, D.-e. Jiang, Y. Chen, Q. Zhang, *Carbon* **2015**, *95*, 1033.
[36] X. L. Sheng, Q. B. Yan, F. Ye, Q. R. Zheng, G. Su, *Phys. Rev. Lett.* **2011**, *106*, 155703.
[37] S. Zhang, J. Zhou, Q. Wang, X. Chen, Y. Kawazoe, P. Jena, *Proc. Natl. Acad. Sci. USA* **2015**, *112*, 2372.
[38] H. Prinzbach, A. Weiler, P. Landenberger, F. Wahl, J. Wörth, L. T. Scott, M. Gelmont, D. Olevano, B. v. Issendorff, *Nature* **2000**, *407*, 60.

[39] Z. Chen, T. Heine, H. Jiao, A. Hirsch, W. Thiel, P. v. R. Schleyer, *Chem. Eur. J.* **2004**, *10*, 963.
[40] X. Zhao, Y. Liu, S. Inoue, T. Suzuki, R. Jones, Y. Ando, *Phys. Rev. Lett.* **2004**, *92*, 125502.
[41] Y. Mao, X. Yan, Y. Xiao, J. Xiang, Y. Yang, H. Yu, *Phys. Rev. B* **2005**, *71*, 033404.
[42] N. Mounet, N. Marzari, *Phys. Rev. B* **2005**, *71*, 205214.
[43] Z.-j. Wu, E.-j. Zhao, H.-p. Xiang, X.-f. Hao, X.-j. Liu, J. Meng, *Phys. Rev. B* **2007**, *76*, 054115.
[44] R. Hill, *Proc. Phys. Soc. London, Sect. A* **1952**, *65*, 349.
[45] R. Andrievski, *Int. J. Refract. Met. Hard Mater.* **2001**, *19*, 447.
[46] S. Pugh, *Phil. Mag.* **1954**, *45*, 823.
[47] C. Y. Zhong, Y. Xie, Y. P. Chen, S. B. Zhang, *Carbon* **2016**, *99*, 65.
[48] M. Zhao, W. Dong, A. Wang, *Sci. Rep.* **2013**, *3*, 3532.
[49] H.-x. Bu, M.-w. Zhao, W.-z. Dong, S.-w. Lu, X.-p. Wang, *J. Mater. Chem. C* **2014**, *2*, 2751.
[50] Y. Yao, F. Ye, X.-L. Qi, S.-C. Zhang, Z. Fang, *Phys. Rev. B* **2007**, *75*, 041401.
[51] P. Chen, F. Huang, S. Yun, *Carbon* **2003**, *41*, 2093.
[52] Y. Tian, Z. Hu, Y. Yang, X. Wang, X. Chen, H. Xu, Q. Wu, W. Ji, Y. Chen, *J. Am. Chem. Soc.* **2004**, *126*, 1180.
[53] H. Feng, J. Ma, Z. Hu, *J. Phys. Chem. C* **2009**, *113*, 16495.
[54] J. Hafner, *From Hamiltonians to Phase Diagrams: The Electronic and Statistical–Mechanical Theory of sp-Bonded Metals and Alloys*, Vol. *70*, Springer Science & Business Media **2012**.

Received: August 30, 2016
Revised: November 26, 2016
Published online: January 12, 2017

